Two-color laser cooling for ^{40}K-^{87}Rb quantum gas mixtures

Yann Kiefer, Max Hachmann, and Andreas Hemmerich*
Institut für Quantenphysik, Universität Hamburg, 22761 Hamburg, Germany;
Zentrum für optische Quantentechnologien, Universität Hamburg, 22761 Hamburg, Germany;
and The Hamburg Centre for Ultrafast Imaging, 22761 Hamburg, Germany

(Received 2 November 2023; accepted 16 January 2024; published 14 February 2024)

We present an efficient cooling scheme for fermionic ^{40}K atoms, using laser light red and blue detuned with respect to the D2 and D1 principle fluorescence lines, respectively. The cooling scheme is found to significantly increase the saturation level for loading of a ^{40}K magneto-optical trap (MOT), resulting in increased atom numbers or decreased cycle times. While the attainable ^{40}K atom number is approximately doubled if exclusively ^{40}K atoms are cooled, the scheme is particularly powerful for dual-species MOTs, for example, if ^{40}K and ^{87}Rb atoms are cooled simultaneously in the same MOT configuration. The typical atom losses due to light-assisted heteronuclear collisions between ^{40}K and ^{87}Rb seem to be reduced, giving rise to a threefold improvement of the ^{40}K atom number as compared to that in a conventional dual-species MOT, operating merely with D2 light. Our scheme can be a useful extension to most dual-species experiments, aiming to reach simultaneous degeneracy of both species.

DOI: 10.1103/PhysRevA.109.023320

I. INTRODUCTION

The recent advances in quantum simulation platforms based on ultracold neutral atoms [1,2] and molecules [3–6] have triggered renewed interest in refined laser cooling techniques enabling rapid cycle times and high fidelity sample preparation [7,8]. To study fundamental low-temperature phases of matter [9,10], degenerate quantum gases are typically employed, requiring temperatures on the 100-nK scale, well below the degeneracy temperature T_{deg}, where the behavior of matter is governed by quantum mechanics. The usual initial step for preparation of a single-species quantum degenerate gas is laser cooling to temperatures below the Doppler temperature T_D (on the order of 100 μK) in a three-dimensional (3D) magneto-optical trap (MOT) [11], which combines an optical molasses [12] with a 3D magnetic quadrupole field. If more than a single atomic species is required, for example, for the production of ultracold heteronuclear molecules, the simultaneous, spatially overlapped operation of multiple 3D MOTs is necessary, referred to as a dual-species 3D MOT. This typically comes with undesirable density and atom number limitations due to two-body loss processes such as molecule association via light assisted collisions in presence of photons of the cooling light [13]. In this paper we present a cooling scheme in a dual-species 3D MOT, which mitigates such losses for the specific case of a ^{40}K-^{87}Rb mixture [14,15].

A possible way to decrease such losses is the use of the *spontaneous force optical trap* (SPOT) technique discussed in Ref. [16]. This method requires one to place a shadow into the repumping beam blocking the light from irradiating the atoms in the trap center. As a result since the cooling cycling transition for alkali-metal atoms is typically not completely closed, the atoms in the trap center naturally accumulate in a dark state and exit the cooling cycle. Hence, the overall fluorescence and the rate of light-assisted collisions decrease. Unfortunately, the SPOT technique is only efficient for rather incompletely closed cycling transitions as in the case of sodium. Hence, it also does not apply for many dual-species mixtures of interest. For single-species scenarios, more recently, laser cooling using multiple atomic transitions was employed and found favorable for improved 3D MOT performance in experiments of alkali-metal [17] and alkaline-earth isotopes [18]. In these works, the improved performance is linked to shielding effects due to short-lived metastable intermediate states.

In the present paper, we explore a two-color scheme for cooling a dual-species ^{40}K-^{87}Rb mixture, where in addition to the conventional laser radiation, detuned to the red side of the D2 transition of ^{40}K at 767 nm, we include a second spectral component, detuned to the blue side of the D1 transition of ^{40}K at 770 nm. The second species, ^{87}Rb , is cooled by the conventional single-color method using red-detuned light on the D2 transition of ^{87}Rb at 780 nm. After introducing the baseline scenario of a single-color, single-species ^{40}K 3D MOT, we benchmark the performance of the two-color cooling scheme in a single-species ^{40}K 3D MOT in the saturated regime. Here, we find an approximately twofold improvement of the number of cooled atoms, as compared to the conventional single-color laser cooling scheme [19]. Subsequently, by adding a conventional single-color 3D MOT for ^{87}Rb , we investigate the dual-species (^{40}K-^{87}Rb) 3D MOT performance when the two-color cooling scheme is applied, finding an up to threefold improvement of the final potassium atom

*hemmerich@physnet.uni-hamburg.de

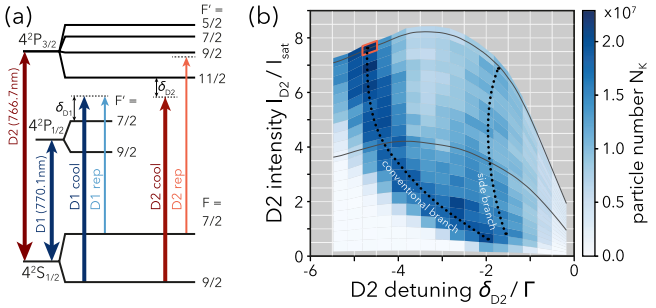

FIG. 1. In (a), the electronic level scheme of ^{40}K is shown. The thick red (blue) arrows indicate the D2 (D1) cooling transitions. The thin arrows indicate the respective repumping transitions. The frequencies of the respective transitions are indicated by their detunings from resonance $\delta_{D2} < 0$ and $\delta_{D1} > 0$. In (b), the ^{40}K atom number, after loading during $t_{load,K} = 3$ s, is plotted against the intensity I_{D2} of the D2 cooling light and the D2 frequency detuning δ_{D2}. The solid gray lines indicate two intensities $I_{D2} = I_{max}$ (upper) and $I_{D2} = 0.5\, I_{max}$ (lower). Black dotted lines are a guide to the eye to indicate the two regimes; see main text

number, which we attribute to the suppression of light-assisted heteronuclear collisions.

II. EXPERIMENTAL SETUP

A. General setup

The experimental setup consists of a dual-species 3D MOT formed by the superposition of single-species MOTs for ^{40}K and ^{87}Rb inside an ultrahigh vacuum (UHV) glass cell. The dual-species 3D MOT is loaded by cold atomic beams of ^{40}K and ^{87}Rb atoms obtained from two separated source regions, which connect to the glass cell via differential pumping stages. The preparation of the cold beams is achieved in so-called 2D$^+$ MOTs, loaded from dispensers. Essentially, this is a two-dimensional (2D) MOT using a magnetic field with linear quadrupole geometry and two additional beams along the zero magnetic field axis, which is referred to by the "+" sign in the acronym. A detailed description of this technique is found in Ref. [20].

B. 2D$^+$ MOTs

The operating parameters of the 2D$^+$ MOTs can be found in Tables I (^{40}K) and II (^{87}Rb) of Appendix A and are not varied throughout all experiments presented in this paper. The rubidium 2D$^+$ MOT is operated on the $5^2S_{1/2} \rightarrow 5^2P_{3/2}$ transition (D2). The frequency of the cooling light is tuned to the red side ($\delta < 0$) of the $|F = 2\rangle \rightarrow |F' = 3\rangle$ transition, while the frequency of the repumping light (required to prepare a closed excitation cycle) is resonant to the $|F = 1\rangle \rightarrow |F' = 0\rangle$ transition. The potassium 2D$^+$ MOT is operated on the $4^2S_{1/2} \rightarrow 4^2P_{3/2}$ transition (D2), with the cooling light tuned to the red side of the $|F = 9/2\rangle \rightarrow |F' = 11/2\rangle$ transition and the repumping light adjusted in resonance with the $|F = 7/2\rangle \rightarrow |F' = 9/2\rangle$ transition. This is indicated by the red arrows in Fig. 1(a), where the electronic level scheme of ^{40}K is shown. For both species, the circular polarization of the cooling and repumping light in the 2D$^+$ MOTs is orthogonal. The intensity ratios I_{cool}/I_{rep} of the cooling and the repumping light in the 2D$^+$ MOTs are 10 for ^{87}Rb and 1 for ^{40}K .

C. ^{87}Rb 3D MOT

The ^{87}Rb 3D MOT uses the same single-color cooling scheme as the ^{87}Rb 2D$^+$ MOT. Similarly to the parameters of both 2D$^+$ MOTs, the parameters of the ^{87}Rb 3D MOT are not varied for all experiments reported here, in order to reduce complexity. The intensity ratio of the cooling and the repumping light for ^{87}Rb is $I_{cool}/I_{rep} = 100$. The magnetic quadrupole field centered around the position of the atoms is realized with a pair of water-cooled copper coils placed outside the vacuum system.

D. ^{40}K 3D MOT

To realize the two-color cooling scheme, the ^{40}K 3D MOT beams are derived from three tapered amplifiers (TAs), divided into six beams of equal intensity delivered by polarization maintaining optical fibers. The cooling and repumping light on the D2 transition is provided by two separate TAs. The cooling and repumping scheme on the D1 transition is realized by a single TA, where the phase-coherent repumping light is imprinted by an electroacoustic modulator operating at $f_{HFS,^{40}K} = 1.285$ GHz [21]. The intensity ratios of the cooling and the repumping light are $I_{cool,D1}/I_{rep,D1} = 10$ and $I_{cool,D2}/I_{rep,D2} = 25$, respectively. For both, ^{87}Rb and ^{40}K 3D MOTs, the amount of repumping light was found to be insensitive with respect to the particle number, if above a certain threshold.

III. SINGLE-SPECIES ^{40}K MOT

To assess the performance of the two-color cooling scheme, for comparison, we first characterize the operation of a conventional single-color, single-species MOT of ^{40}K atoms. In Fig. 1(b), we plot the ^{40}K particle number as a function of the D2 cooling light intensity I_{D2} and the D2 cooling light frequency detuning δ_{D2} for a loading time of $t_{load,K} = 3$ s obtained by absorption imaging.

In this plot, we identify two different domains, which are clearly separated for $I_{D2} > 3\, I_{sat}$.

The first domain (*conventional branch*) is found around $\delta_{D2} < -4\,\Gamma$ and $I_{D2} > 3\, I_{sat}$ (large negative detuning and large intensity) denoted by the black dotted line, which serves as a guide to the eye. Here, we find the maximum particle number of $N_K = 2.2 \times 10^7$ for $\delta_{D2} = -3.5\,\Gamma$ and $I_{D2} = I_{D2,max} = 7.5\, I_{sat}$ [red rectangle in Fig. 1(b)]. The second domain (*side branch*) is found for more resonant D2 cooling light frequency detuning $\delta_{D2} \approx -2\,\Gamma$ at almost all settings of the intensity I_{D2}. Here, we find particle numbers up to $N_K = 1.5 \times 10^7$. Between these two domains we observe a local minimum of the particle number N_K. While for the single-color scheme, the second domain of the ^{40}K 3D MOT shows slightly less efficient performance, this domain becomes relevant if the two-color operation of the MOT is investigated.

In contrast to conventional laser cooling in a MOT, we additionally employ blue-detuned light on the D1 transition of ^{40}K as indicated by the set of blue arrows in Fig. 1(a), similar to the experiments presented in [17] and reminiscent

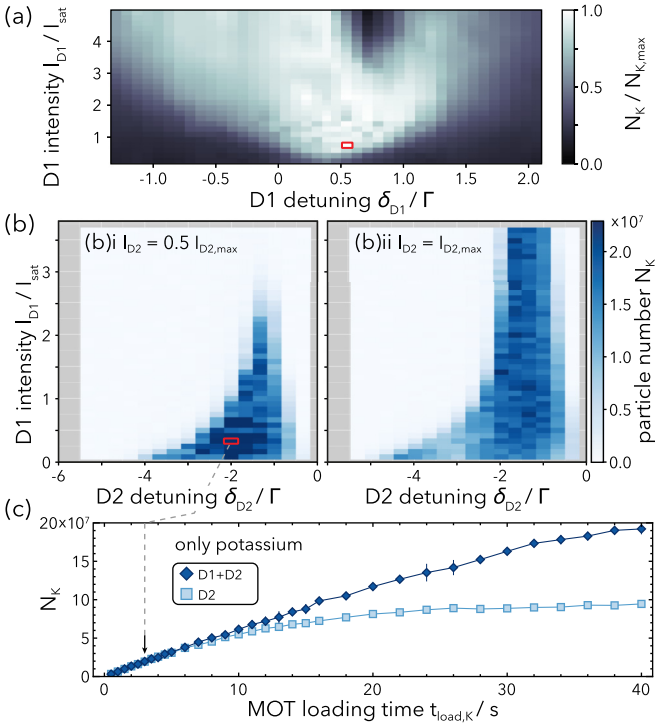

FIG. 2. In (a), the normalized ^{40}K atom number $N_K/N_{K,max}$ is plotted against the D1 cooling light intensity I_{D1} and the cooling light detuning δ_{D1}. In (b), the ^{40}K atom number N_K after $t_{load} = 3$ s is plotted against the D2 cooling light detuning δ_{D2} and the D1 intensity I_{D1} for two distinct settings of the D2 intensity $I_{D2} = 0.5 I_{D2,max}$ (i) and $I_{D2} = I_{D2,max}$ (ii). In (a) and (b), the red rectangle indicates the parameter settings where the maximal ^{40}K atom number is found. In (c), N_K is plotted against the loading time $t_{load,K}$. The light blue squares show N_K for optimal parameters according to Fig. 1(b), when only the D2 transition is used for cooling. The dark blue diamonds show N_K for cooling on both D1 and D2 transitions for optimal parameters denoted by the black arrow and the red square in (b).

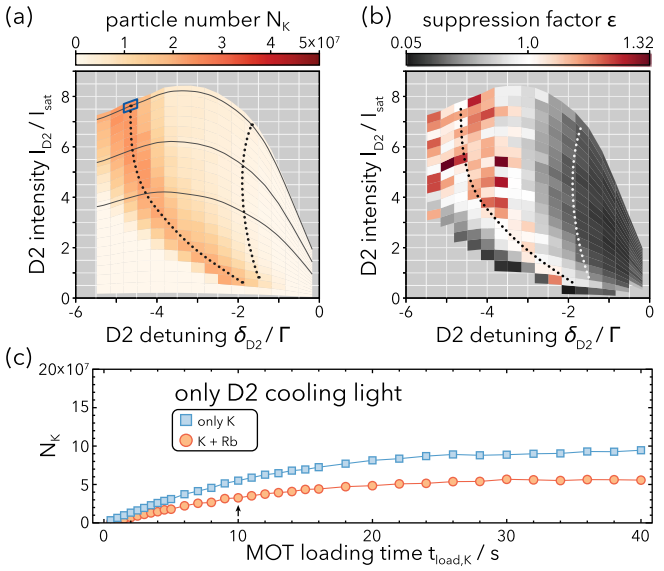

FIG. 3. In (a), the potassium atom number is plotted as a function of the intensity I_{D2} and the frequency detuning δ_{D2} in the dual-species MOT in absence of any cooling light operating on the D1 transition. In (b), we plot the suppression factor ε defined as the ratio of the normalized particle numbers N_K found for single- and dual-species MOT operation. In (c), we plot the particle number N_K of the single-species (light blue squares) and the dual-species (orange circles) MOT as a function of the loading time $t_{load,K}$. The blue square in (a), close to the upper left corner, indicates the optimal parameters used for measuring the loading curve in (c). The black arrow in (c) indicates the loading time for which (a) is obtained.

of VSCPT [22] and gray molasses cooling [23]. In Fig. 2(a), we plot the normalized potassium particle number $N_K/N_{K,max}$ as a function of the D1 detuning δ_{D1} and the D1 intensity I_{D1}. In this experiment we fix the parameters of the D2 cooling light to $I_{D2} = 5.76\, I_{sat}$ and $\delta_{D2} = -1.67\,\Gamma$ (optimal values according to Fig. 4). We identify two regimes separated by a local minimum around $I_{D1} > 3\, I_{sat}$ and $0.4\,\Gamma < \delta_{D1} < 1.0\,\Gamma$. Our qualitative understanding of these domains of optimal performance is limited and a subject of further investigation. The parameter setting for optimal MOT performance of the D1 frequency detuning $\delta_{D1} = 0.55\,\Gamma$ is indicated by the red rectangle in Fig. 2(a) and is kept at this value for all following investigations.

First, we vary the intensity I_{D1} of the D1 cooling light and the detuning δ_{D2} of the D2 cooling light for two different settings of the intensity I_{D2} of the D2 cooling light, as can be seen in Fig. 2(b). The intensity of the D2 cooling light is set $I_{D2} = 0.5\, I_{D2,max}$ in Fig. 2(b)i and to $I_{D2} = I_{D2,max}$ in Fig. 2(b)ii according to the solid gray lines in Fig. 1(b). The color map is set to be identical to the color map in Fig. 1(b), so that the saturated data points correspond to an improved MOT performance. We observe that with the inclusion of cooling light operating on the D1 transition of ^{40}K , the optimal setting of the D2 cooling frequency detuning is at $\delta_{D2} = -2\,\Gamma$ in contrast to the optimal detuning without cooling on the D1 transition, which is found to be $\delta_{D2} = -4.65\,\Gamma$. Additionally, we have varied the ratio of the intensities I_{D1}/I_{D2}. If $I_{D2} = I_{D2,max}$ [see Fig. 2(b)ii], I_{D1} can be set to larger values and still yield reasonable ^{40}K MOT atom numbers. However, we find the best performance for parameter settings $I_{D2} = 0.5\, I_{D2,max}$, $I_{D1} = 0.33\, I_{sat}$, and $\delta_{D2} = -2\Gamma$ according to the data point indicated with a red rectangle in Fig. 2(b)i. Here, we obtain $N_K = 2.51 \times 10^7$ after $t_{load,K} = 3$ s, a 13 % improvement compared to the single-color operation, as indicated by the black arrow in Fig. 2(c).

As a last step, we investigate the ^{40}K atom number N_K as a function of the MOT loading time t_{load} shown in Fig. 2(c). For this, we load the MOT for variable times at optimal parameters indicated by the rectangles both for the D2 only MOT [see Fig. 1(b)] and the two-color MOT [see Fig. 2(b)i]. For short loading times of $t_{load,K} < 8$ s the improvement by the two-color cooling scheme is marginal. However, for longer loading times $t_{load,K} > 8$ s an almost twofold increase of the ^{40}K atom number N_K is obtained. To extrapolate the saturation levels of the two cooling methods, we fit both data sets in Fig. 2(c) with a time dependent rate equation model, including a density dependent two-body loss term [24], and find a threefold increased saturation level in the two-color scenario. The loading curve is found to be well fitted by this model, indicating that, in contrast to the single-color MOT, even larger atom numbers

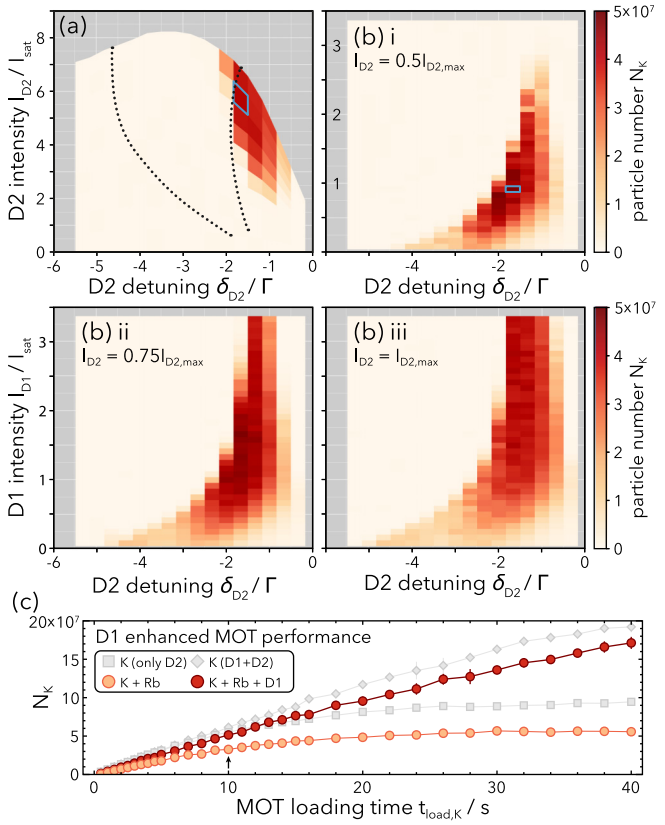

FIG. 4. In (a), N_K is shown as a function of the intensity I_{D2} and the frequency detuning δ_{D2} for a fixed value of $I_{D1} = 1.5\, I_{sat}$. In (b), N_K is plotted as a function of the intensity I_{D1} and the frequency detuning δ_{D2} for a fixed value of $I_{D2} = 0.5$ (i), 0.75 (ii), and 1.00 (iii) $\times$ $I_{D2,max}$. In (a) and (b), the blue rectangles denote the optimal MOT operation parameters. In (c), N_K is plotted vs the loading time $t_{load,K}$ for the respective optimal parameters of each cooling method. The optimal parameter for the two-color cooling scheme is indicated by the blue rectangle in panel (b)i. The red circles denote N_K in a dual-species MOT with cooling on both the D1 and the D2 transition. The orange circles denote N_K in a dual-species MOT with conventional cooling only on the D2 transition. The gray diamonds (squares) correspond to loading curves previously obtained in Fig. 2(c) [Fig. 3(c)].

can be expected, by increasing the flux of the cold ^{40}K beam source. See Appendix B for details of the fit model.

So far the only discussed parameter was the particle number N_K of the potassium MOT; however, the second relevant parameter which is of importance is the temperature T of the atomic ensemble. We have measured the temperature for cooling parameters according to Fig. 2(c) and found it to be weakly dependent. A discussion of the ensemble temperatures for all applied cooling schemes can be found in Appendix C.

IV. SINGLE-COLOR DUAL-SPECIES MOT

In this section, we investigate the negative effects of light-assisted heteronuclear collisions (LAHNCs) on the performance of a dual-species MOT for ^{40}K and ^{87}Rb atoms, operating with conventional single-color D2 only cooling. Since the loading efficiency of rubidium is much larger than that of potassium, we apply different loading times for both species. Typically, we operate with a variable loading time $t_{load,K}$ for ^{40}K atoms followed by a time window with a duration $t_{load,KRb} = 3$ s, during which both species ^{40}K and ^{87}Rb are loaded. The rubidium atom number N_{Rb} that is obtained after $t_{load,KRb} = 3$ s is identical for all dual-species scenarios and is $N_{Rb} = 1.5 \times 10^9$. During the combined loading period $t_{load,KRb}$ we see no further increase of the ^{40}K atom number N_K but rather a decrease attributed to LAHNCs. In order to consistently compare loading of ^{40}K atoms with loading of ^{40}K and ^{87}Rb atoms, we equally specify the ^{40}K atom number N_K and the loading time $t_{load,K}$ for both cases.

In Fig. 3(a), we plot the ^{40}K atom number N_K as a function of the intensity I_{D2} and the detuning δ_{D2} of the D2 cooling light. In the conventional branch, we observe a similar qualitative behavior as previously found in Fig. 1(b) for the single-species D2 only MOT. In Fig. 3(a), the maximum particle number $N_K = 2.38 \times 10^7$ is found in the conventional branch for a detuning $\delta_{D2} = -4.6\,\Gamma$ and an intensity of $I_{D2} = 7.7\, I_{sat}$. However, the side branch obtained in Fig. 1(b), vanishes. We explain this behavior with an increased photon scattering for cooling light tuned closer to the atomic resonance ($\delta_{D2} \approx 0$), which in consequence leads to pronounced LAHNCs and associated two-body loss.

To further illustrate the impact of the presence of rubidium atoms on the potassium atom number N_K, we plot the suppression factor ε in Fig. 3(b), which is defined as the ratio of the normalized ^{40}K atom numbers for the single-species (Fig. 1) and the dual-species [Fig. 3(a)] single-color ^{40}K MOT, i.e., both in absence of D1 cooling. The red shaded areas in Fig. 3(b) (suppression factor $\varepsilon > 1$) indicate regions, where the dual-species MOT performs better compared to the single-species case, whereas the black areas ($\varepsilon < 1$) denote the regions where the N_K is severely reduced by the presence of ^{87}Rb atoms.

In Fig. 3(c), we investigate N_K as a function of the loading time $t_{load,K}$. The orange circles denote N_K for optimal parameters indicated by the blue rectangle in Fig. 3(a). For comparison, the blue squares repeat N_K found in Fig. 2(c) for the single-species single-color scenario. We see that the ^{40}K atom number for the single-color dual-species MOT is clearly reduced due to the presence of ^{87}Rb atoms. The black arrow in Fig. 3(c) marks the loading time $t_{load,K} = 10$ s, for which Fig. 3(a) is obtained.

V. TWO-COLOR, DUAL-SPECIES MOT

Adding blue-detuned light on the D1 transition significantly improves the dual-species MOT performance. This central result is analyzed in the remainder of this paper.

In Fig. 4(a), we investigate the effects of additional cooling light operating on the D1 transition with an intensity of $I_{D1} = 1.5\, I_{sat}$ in a dual-species MOT of ^{40}K and ^{87}Rb . This extends the previous investigations of D1 line cooling in a single-species MOT for ^{40}K shown in Fig. 2. To compare our results to the previous measurements in Figs. 1(b), 2, and 3(a), we vary the intensity I_{D2} and the frequency detuning δ_{D2} and count the ^{40}K atom number N_K. We observe a notably different behavior throughout the entire measured parameter regime. The previously dominant conventional branch no longer appears. Surprisingly, we find that the inclusion of the

D1 cooling light restores the side branch and even enhances the particle number N_K above the saturation threshold found for the D2 only dual-species MOT, as can clearly be seen in Fig. 4(a). In absence of D1 cooling, this parameter region is subject to significant LAHNCs and consequently low potassium particle numbers N_K. Note that the color map in Figs. 3 and 4 is equal, displaying a significantly larger ^{40}K MOT in presence of D1 cooling. In Fig. 4(b), we vary the D1 intensity I_{D1} and the D2 detuning δ_{D2} for three distinct settings of the D2 intensity I_{D2} as indicated by the insets. We observe a similar behavior as compared to the single-species MOT and find that the performance of the MOT is sensitive to the relative powers of I_{D1} and I_{D2}. We obtain a maximum number of 5×10^7 in the case of the two-color dual-species MOT ($I_{D1} = 0.91\, I_{sat}$ and $\delta_{D2} = -1.67\, \Gamma$) for a parameter setting indicated by the blue rectangle in Fig. 4(b)i. This corresponds to a twofold increase for $t_{load,K} = 10$ s compared to the conventional single-color dual-species D2 MOT number obtained in Fig. 3(a). Finally, we plot the potassium atom number N_K of the dual-species MOT versus the loading time t_{load} in Fig. 4(c). Here, the red circles denote N_K in the two-color dual-species MOT. The orange circles mark N_K for the single-color dual-species configuration of the MOT [see Fig. 3(c)]. The gray data, for comparison, repeat the data shown in Fig. 2(c).

For short loading times $t_{load,K} < 3$ s, the two cooling methods yield comparable results. However, for longer loading times $t_{load,K} > 3$ s the potassium atom number N_K is significantly increased by the implementation of the two-color cooling. For the longest loading times investigated in our experiment, we find $N_K = 1.71 \times 10^8$ for the two-color cooling scheme and $N_K = 5.67 \times 10^7$ for the single-color case. This is a threefold improvement in the dual-species scenario. From the behavior of the loading curve it is a reasonable assumption that the improvement can be even more significant for longer loading times as the ^{40}K atom number N_K in the single-color MOT is saturated after ≈15 s, while the reach of saturation of the potassium number in the two-color cooling scheme is significantly shifted towards later times (see Appendix B).

VI. CONCLUSION

In summary, we demonstrate a powerful cooling scheme for preparing mixtures of cold ^{40}K and ^{87}Rb atoms in a dual-species MOT. In addition to the conventional cooling of ^{40}K atoms using light tuned to the red side of the D2 transition, a second light component, tuned to the blue side of the D1 transition, is used. We have started with benchmarking the performance of a conventional single-species MOT for ^{40}K atoms using single frequency cooling light with a negative detuning $\delta_{D2} < 0$ with respect to the D2 line and an intensity I_{D2}. Two domains in the parameter space $\{\delta_{D2}, I_{D2}\}$ are identified, dubbed *conventional branch* and *side branch*, where the cooling efficiency attains a relative maximum, while the global maximum is reached in the conventional branch. In a second step, discussed in Sec. III, we demonstrate that the inclusion of additional light beams, blue detuned with respect to the D1 transition, can increase the potassium atom number in a single-species MOT for long loading times. In a third step, we investigate MOT loading in a dual-species scenario of ^{40}K and ^{87}Rb . In Sec. IV, we benchmark the dual-species MOT using conventional cooling on the D2 transition. Here, we find significant atomic losses due to LAHNCs and the disappearance of the side branch. Finally, in Sec. V, we investigate the influence of the two-color cooling scheme in a dual-species MOT scenario. We observe a significant improvement of the ^{40}K atom number N_K, with the side branch forming the optimal parameter region. For long MOT loading times we demonstrate a threefold improvement of N_K. We attribute the significant reduction of saturation of ^{40}K loading, observed in the dual-color MOT, to a suppression of light-assisted heteronuclear collisions between ^{40}K and ^{87}Rb atoms. We believe that this is due to optical pumping and the resulting population of dark states. As a consequence, longer loading times or an increase of the flux of the cold ^{40}K beam source allow for larger N_K. Due to the similar level structure of alkali-metal atomic species, we suspect that the discussed cooling scheme can be a useful extension for most modern dual-species alkali-metal quantum gas experiments, which require high fidelity preparation of large atomic samples with high repetition rates.

ACKNOWLEDGMENTS

We acknowledge support from the Deutsche Forschungsgemeinschaft through the collaborative research center SFB 925 (Project No. 170620586, C1). M.H. was partially supported by the Cluster of Excellence CUI: Advanced Imaging of Matter of the Deutsche Forschungsgemeinschaft through EXC 2056 (Project No. 390715994).

APPENDIX A: 2D MOT PARAMETERS

In the source region, separated from the main chamber by a differential pumping stage, a room-temperature thermal alkali-metal vapor is precooled to produce a collimated cold atomic beam. To increase the pressure of the alkali-metal gas, UV-LEDs are operated simultaneously with the loading phase. This method has been shown to increase the loading rates of alkali-metal MOTs [25]. In our apparatus, the loading rate is increased almost up to tenfold using this technique [26]. The loading rate was found to be proportional to the intensity of the UV light.

In our case, the 2D$^+$ MOT is formed by two pairs of counterpropagating laser beams in a retroreflected configuration. These pairs of beams are used for transverse cooling of the particles. These four beams, together with a magnetic quadrupole field, form a conventional 2D MOT. In our setup, however, there is an extension of this scheme, namely an additional cooling beam aligned perpendicular to the two

TABLE I. Experimentally optimized ^{40}K 2D+ MOT parameters.

Parameter	Transversal	Axial
Magnetic gradient	17.5 G cm^{-1}	0 G cm^{-1}
$1/e$ beam diameter	26.9 mm	14.4 mm
I_{cool} per beam	28 I_{sat}	70 I_{sat}
I_{rep} per beam	27.5 I_{sat}	14 I_{sat}
δ_{cool}	$-3\,\Gamma$	$-3.6\,\Gamma$
δ_{rep}	$-0.05\,\Gamma$	$-0.05\,\Gamma$

TABLE II. Experimentally optimized ^{87}Rb 2D+ MOT parameters.

Parameter	Transversal	Axial
Magnetic gradient	14 G cm^{-1}	0 G cm^{-1}
$1/e$ beam diameter	26.9 mm	10.8 mm
I_{cool} per beam	8 I_{sat}	20 I_{sat}
I_{rep} per beam	0.3 I_{sat}	0 I_{sat}
δ_{cool}	$-2.7\,\Gamma$	$-2.7\,\Gamma$
δ_{rep}	$0\,\Gamma$	

TABLE III. Experimentally optimized ^{87}Rb 3D MOT parameters.

Parameter	Transversal
Magnetic gradient	7.5 G cm^{-1}
$1/e$ beam diameter	26.9 mm
I_{cool} per beam	1.7 I_{sat}
I_{rep} per beam	0.04 I_{sat}
δ_{cool}	$-2.7\,\Gamma$
δ_{rep}	$0\,\Gamma$

transversal beams, called the axial cooling beam (hence the designation 2D$^+$ MOT). This axial beam is reflected from the surface of a substrate located inside the UHV system, which has a small hole to allow the transfer of the precooled atoms into the main chamber through a differential pumping stage. The 2D$^+$ MOT operates only on the D2 line of ^{40}K and therefore addresses the $|F = 9/2\rangle \rightarrow |F' = 11/2\rangle$ transition for cooling and the$|F = 7/2\rangle \rightarrow |F' = 9/2\rangle$ transition for repumping of the atoms [see Fig. 1(a)]. The magnetic quadrupole field to generate the transversal magnetic confinement is provided by two pairs of coils placed outside the UHV source region. Static stray magnetic fields are compensated by additional coil pairs in the transversal direction. This magnetic field infrastructure allows for magnetic gradients up to 20 G/cm and homogeneous magnetic compensation fields on the order of several G. The experimentally optimized parameters of the 2D$^+$ MOT can be found in Table I. Efficient operation of the 2D$^+$ MOT is a crucial step in the experiments, since the atomic flux determined by the quality of the 2D$^+$ MOT strongly influences the performance of the 3D MOT and thus all subsequent steps in the production of cold atoms.

The rubidium 2D$^+$ MOT is realized in the same configuration as the potassium 2D$^+$ MOT. The experimentally optimized parameters of the ^{87}Rb 2D$^+$ MOT can be found in Table II. The experimentally optimized parameters of the ^{87}Rb and ^{40}K 3D MOT can be found in Table III. The parameter values presented in the Appendix A are not varied throughout the series of experiments described in the main text.

APPENDIX B: LONG-TERM MOT LOADING BEHAVIOR

To gain insights about the long-term loading behavior of the different MOT loading scenarios, we fit our experimental data obtained in the main text [Figs. 2(c) and 4(c)] to a rate equation model commonly utilized describing the loading behavior of single-species MOTs [27,28]:

$$\frac{\partial N_x(t)}{\partial t} = R - \gamma N_x(t) - \beta_x N_x(t)^2 \tag{B1}$$

where $N_x(t)$ denotes the particle number N_{K} found in the single-color ($x = \mathrm{D2}$) or dual-color ($x = \mathrm{D1D2}$) operation. We extract the constant atomic loading rate R and the single-particle loss rate γ with a simultaneous fit to both loading curves shown in Fig. 5(a). The additional free parameter β_x models the density-dependent loss rate, which is assumed to be different between the two scenarios and is therefore individually determined. We find that the ratio of the density-dependent loss rate $\beta_{\mathrm{D2}}/\beta_{\mathrm{D1D2}} = 9.7(20)$ is far from unity, resulting in a vastly different saturation level in both cases. Extrapolating these loading curves beyond the measured loading duration to times of up to $t_{\mathrm{load,K}} < 180\,\mathrm{s}$ leads to a difference in the saturation level of 2.96(9) as can be seen in Fig. 5(c).

In the dual-species setting, isolating individual processes is much more challenging and therefore the loading behavior can no longer be captured with a simple rate equation model. The inclusion of an additional inter-species density-dependent loss term fails to accurately describe the experimental data. In Fig. 5(b), we plot the potassium atom number N_{K} of the

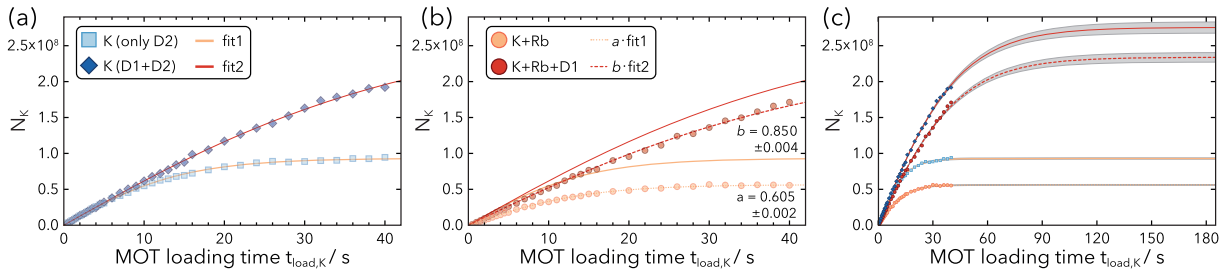

FIG. 5. In (a), we repeat the data obtained in the main text of this paper of the single-species MOT (Fig. 2) and plot the potassium atom number N_{K} as a function of the loading time $t_{\mathrm{load,K}}$. In (a), the salmon and red solid line denotes the fit of the single-species data according to the correct model for the single-color and two-color MOT, respectively. For details, see text in Appendix B. In (b), we repeat the data obtained in the main text of the dual-species MOT (Fig. 4) and plot the potassium atom number N_{K} as a function of the loading time $t_{\mathrm{load,K}}$. Here, the dotted lines denote a fit according to the insets, where the curves fit1 and fit2 are scaled by fitted factors $a = 0.605(2)$ (salmon) and $b = 0.850(4)$ (red), respectively. In (c), we investigate the predicted loading behavior of the four scenarios according to the models in the text. The data of (a) and (b) and the solid lines denote the fit according to the model in Eq. (B1). The gray shaded areas denote the 99 % confidence intervals of the fit.

dual-species MOT as a function of the loading time $t_{\mathrm{load,K}}$. The solid lines repeat the fits obtained in Fig. 5(a) for comparability. Interestingly we find that the data are best modeled by rescaling the previously determined fit functions fit 1 and fit 2 with factors $a = 0.605(2)$ and $b = 0.850(4)$, respectively. Once again, extrapolating beyond the measured data, we obtain a difference in saturation level of $2.96(9) \times b/a = 4.16(13)$ as can be seen in Fig. 5(c). However, without access to the correct rate equation models, this result has to be taken with care.

APPENDIX C: TEMPERATURE OF THE MOT

The ensemble temperature is a relevant property to discuss in experiments concerned with laser cooling methods. We have purposely limited its discussion in the main text as we have found very weak dependence of the MOT temperature with respect to the applied cooling method. We have measured the temperature for the four investigated cooling methods operated at their respective optimal parameters and visualized in Fig. 6. We generally observe temperatures slightly below the Doppler temperature $T_{\mathrm{Doppler}} = 145\,\mu\mathrm{K}$ which is usually sufficient as in most modern cold atom experiments

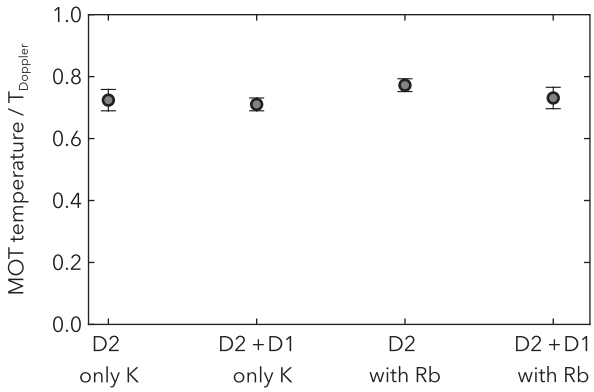

FIG. 6. Temperature of the ^{40}K MOT after $t_{\mathrm{load,K}} = 10\,\mathrm{s}$ for the four discussed cooling schemes in units of the Doppler temperature T_{Doppler}. The errors bars denote the uncertainties of the fitting routine.

the MOT phase is followed by a sequence of sub-Doppler cooling schemes such as (gray) molasses cooling. Therefore, the optimization of the MOT parameters prioritizes the captured number of particles N_{K} over other relevant quantities such as the temperature or density.

[1] J. F. Sherson, C. Weitenberg, M. Endres, M. Cheneau, I. Bloch, and S. Kuhr, Single-atom-resolved fluorescence imaging of an atomic Mott insulator, Nature (London) **467**, 68 (2010).

[2] A. Mazurenko, C. S. Chiu, G. Ji, M. F. Parsons, M. Kanász-Nagy, R. Schmidt, F. Grusdt, E. Demler, D. Greif, and M. Greiner, A cold-atom Fermi-Hubbard antiferromagnet, Nature (London) **545**, 462 (2017).

[3] L. D. Marco, G. Valtolina, K. Matsuda, W. G. Tobias, J. P. Covey, and J. Ye, A degenerate Fermi gas of polar molecules, Science **363**, 853 (2019).

[4] A. Schindewolf, R. Bause, X.-Y. Chen, M. Duda, T. Karman, I. Bloch, and X.-Y. Luo, Evaporation of microwave-shielded polar molecules to quantum degeneracy, Nature (London) **607**, 677 (2022).

[5] I. Stevenson, A. Z. Lam, N. Bigagli, C. Warner, W. Yuan, S. Zhang, and S. Will, Ultracold gas of dipolar nacs ground state molecules, Phys. Rev. Lett. **130**, 113002 (2023).

[6] Y. Kiefer, M. Hachmann, and A. Hemmerich, Ultracold Feshbach molecules in an orbital optical lattice, Nat. Phys. **19**, 794 (2023).

[7] H. Bernien, S. Schwartz, A. Keesling, H. Levine, A. Omran, H. Pichler, S. Choi, A. S. Zibrov, M. Endres, M. Greiner, V. Vuletić, and M. D. Lukin, Probing many-body dynamics on a 51-atom quantum simulator, Nature (London) **551**, 579 (2017).

[8] M. O. Brown, S. R. Muleady, W. J. Dworschack, R. J. Lewis-Swan, A. M. Rey, O. Romero-Isart, and C. A. Regal, Time-of-flight quantum tomography of an atom in an optical tweezer, Nat. Phys. **19**, 569 (2023).

[9] F. Schäfer, T. Fukuhara, S. Sugawa, Y. Takasu, and Y. Takahashi, Tools for quantum simulation with ultracold atoms in optical lattices, Nat. Rev. Phys. **2**, 411 (2020).

[10] L. Chomaz, I. Ferrier-Barbut, F. Ferlaino, B. Laburthe-Tolra, B. L. Lev, and T. Pfau, Dipolar physics: A review of experiments with magnetic quantum gases, Rep. Prog. Phys. **86**, 026401 (2023).

[11] E. L. Raab, M. Prentiss, A. Cable, S. Chu, and D. E. Pritchard, Trapping of neutral sodium atoms with radiation pressure, Phys. Rev. Lett. **59**, 2631 (1987).

[12] J. Dalibard and C. Cohen-Tannoudji, Laser cooling below the Doppler limit by polarization gradients: Simple theoretical models, J. Opt. Soc. Am. B **6**, 2023 (1989).

[13] M. H. Anderson, W. Petrich, J. R. Ensher, and E. A. Cornell, Reduction of light-assisted collisional loss rate from a low-pressure vapor-cell trap, Phys. Rev. A **50**, R3597 (1994).

[14] J. Goldwin, S. B. Papp, B. DeMarco, and D. S. Jin, Two-species magneto-optical trap with ^{40}K and ^{87}Rb , Phys. Rev. A **65**, 021402(R) (2002).

[15] S. Ospelkaus-Schwarzer, Quantum degenerate Fermi-Bose mixtures of ^{40}K and ^{87}Rb in 3D optical lattices, Ph.D. thesis, Universität Hamburg, 2006, p. 174.

[16] W. Ketterle, K. B. Davis, M. A. Joffe, A. Martin, and D. E. Pritchard, High densities of cold atoms in a dark spontaneous-force optical trap, Phys. Rev. Lett. **70**, 2253 (1993).

[17] G. Salomon, L. Fouché, P. Wang, A. Aspect, P. Bouyer, and T. Bourdel, Gray-molasses cooling of ^{39}K to a high phase-space density, Europhys. Lett. **104**, 63002 (2013).

[18] J. Höschele, S. Buob, A. Rubio-Abadal, V. Makhalov, and L. Tarruell, Atom-number enhancement by shielding atoms from losses in strontium magneto-optical traps, Phys. Rev. Appl. **19**, 064011 (2023).

[19] B. DeMarco and D. S. Jin, Onset of Fermi degeneracy in a trapped atomic gas, Science **285**, 1703 (1999).

[20] K. Dieckmann, R. J. C. Spreeuw, M. Weidemüller, and J. T. M. Walraven, Two-dimensional magneto-optical trap as a source of slow atoms, Phys. Rev. A **58**, 3891 (1998).

[21] T. Tiecke, Properties of potassium, https://www.tobiastiecke.nl/archive/PotassiumProperties.pdf (2019).

[22] M. Weidemüller, T. Esslinger, M. A. Ol'shanii, A. Hemmerich, and T. W. Hänsch, A novel scheme for efficient cooling below the photon recoil limit, Europhys. Lett. **27**, 109 (1994).

[23] D. Rio Fernandes, F. Sievers, N. Kretzschmar, S. Wu, C. Salomon, and F. Chevy, Sub-Doppler laser cooling of fermionic ^{40}K atoms in three-dimensional gray optical molasses, Europhys. Lett. **100**, 63001 (2012).

[24] J. Grünert and A. Hemmerich, Optimizing the production of metastable calcium atoms in a magneto-optical trap, Appl. Phys. B **73**, 815 (2001).

[25] C. Klempt, T. van Zoest, T. Henninger, O. Topic, E. Rasel, W. Ertmer, and J. Arlt, Ultraviolet light-induced atom desorption for large rubidium and potassium magneto-optical traps, Phys. Rev. A **73**, 013410 (2006).

[26] M. Hachmann, Y. Kiefer, J. Riebesehl, R. Eichberger, and A. Hemmerich, Quantum degenerate Fermi gas in an orbital optical lattice, Phys. Rev. Lett. **127**, 033201 (2021).

[27] T. P. Dinneen, K. R. Vogel, E. Arimondo, J. L. Hall, and A. Gallagher, Cold collisions of Sr*-Sr in a magneto-optical trap, Phys. Rev. A **59**, 1216 (1999).

[28] H. C. Busch, M. K. Shaffer, E. M. Ahmed, and C. I. Sukenik, Trap loss in a dual-species Rb-Ar* magneto-optical trap, Phys. Rev. A **73**, 023406 (2006).